



HAL
open science

A proof-of-concept study of coupled supercritical CO₂-assisted processes to produce solid self-assembled drug delivery systems (S-SADDS)

Thibault Massias, Suenia de Paiva Lacerda, Jacqueline Resende de Azevedo, Jean-jacques Letourneau, Philomène Dos Santos, Marie-Alexandrine Bolzinger, Fabienne Espitalier

► To cite this version:

Thibault Massias, Suenia de Paiva Lacerda, Jacqueline Resende de Azevedo, Jean-jacques Letourneau, Philomène Dos Santos, et al.. A proof-of-concept study of coupled supercritical CO₂-assisted processes to produce solid self-assembled drug delivery systems (S-SADDS). *Journal of Crystal Growth*, 2023, 616, pp.127245. 10.1016/j.jcrysgro.2023.127245 . hal-04111875

HAL Id: hal-04111875

<https://imt-mines-albi.hal.science/hal-04111875>

Submitted on 31 May 2023

HAL is a multi-disciplinary open access archive for the deposit and dissemination of scientific research documents, whether they are published or not. The documents may come from teaching and research institutions in France or abroad, or from public or private research centers.

L'archive ouverte pluridisciplinaire **HAL**, est destinée au dépôt et à la diffusion de documents scientifiques de niveau recherche, publiés ou non, émanant des établissements d'enseignement et de recherche français ou étrangers, des laboratoires publics ou privés.

A proof-of-concept study of coupled supercritical CO₂-assisted processes to produce solid self-assembled drug delivery systems (S-SADDS)

Thibault Massias^{a,b}, Suênia de Paiva Lacerda^a, Jacqueline Resende de Azevedo^b,
Jean-Jacques Letourneau^a, Philomène Dos Santos^a, Marie-Alexandrine Bolzinger^b,
Fabienne Espitalier^{a,*}

^a Centre RAPSODEE, IMT Mines-Albi, UMR CNRS 5302, Université de Toulouse, Albi, France

^b Laboratoire d'Automatique, de Génie des Procédés et de Génie Pharmaceutique, (LAGEPP UMR CNRS 5007), Université Claude Bernard Lyon 1, Villeurbanne, France

A B S T R A C T

The development of innovative drug delivery systems is currently under intense consideration to overcome bioavailability issues of poorly water-soluble drugs. Among the many existing delivery systems, self-assembled drug delivery systems (SADDS) are of great interest. Solid Lipid Nanoparticles (SLN), which are part of SADDS, have been widely studied in the pharmaceutical field since they are biodegradables and biocompatibles. However, stability of SLN suspension over time is limited and quick drug released were frequently observed. The development of solid SADDS (S- SADDS), to produce an on-demand delivery system, through a one-step production process has been designed to overcome these issues. The coupling of both Supercritical Carbon Dioxide (scCO₂) assisted RESS and SAS processes (RESS/SAS) have been proposed as a proof-of-concept. This study was carried out in three steps: (i) the development and adjustment of operating conditions to produce SLN suspension using solvent injection process, (ii) the optimization of the formulation to produce SLN with a mean particle size diameter close to 100 nm and stable at least 24 h, (iii) the transposition of the SLN formulation composition into the RESS/SAS coupled process for the production of S-SADDS. SLN composed of stearic acid, PVP K30, phosphatidylcholine and nifedipine, with an average size under 100 nm and a zeta potential about -35 mV were obtained from the preliminary study. These results allowed the transposition of the optimal formulation into RESS/SAS crystallization process. The developed RESS/SAS scCO₂-assisted processes demonstrate the simultaneous crystallization of a self-assembled formulation in a one step process. A control of operating conditions was also demonstrated through the generation of S- SADDS containing desired amount of nifedipine. The proof-of-concept process studied, seems to be very promising tool for the generation of complex solids, intermediate products or for the development of innovative drug delivery systems.

1. Introduction

The development of innovative drug delivery systems is currently under intense consideration to overcome bioavailability issues of poorly water-soluble active ingredients. Among the many existing delivery systems, self-assembled drug delivery systems (SADDS) are probably the most studied [1,2]. Solid lipid nanoparticles (SLN), which are part of

SADDS, are of great interest in the pharmaceutical field since they are biodegradable and biocompatible [3,4]. In addition, their composition associated with surfactants often allows the generation of particle size below 100 nm. It is regularly described as the optimal size for which nanoparticles are able to interact with cells and reach the therapeutic target more efficiently [5,6]. These specific interactions allowed rapid cellular uptakes through transcytosis pathway from oral administration

Abbreviations: CO₂, Carbon dioxide; DSC, Differential scanning calorimetry; DSL, Dynamic light scattering; EtOH, Ethanol; FTIR, Fourier transform infra-red spectrometry; NIF, Nifedipine; PC, Phosphatidylcholine; PDI, Polydispersity index; PVP, Polyvinylpyrrolidone; RESS, Rapid expansion of supercritical solution; RESS/SAS, Coupled RESS and SAS processes; SADDS, Self-assembled drug delivery system; SAS, Supercritical antisolvent; scCO₂, Supercritical carbon dioxide; SD, Standard deviation; SEM, Scanning electron microscopy; SLN, Solid lipid nanoparticle; S-SADDS, Solid self-assembled drug delivery system; VA, Vinyl acetate; XRPD, X-Ray powder diffraction.

* Corresponding author at: RAPSODEE, Research Centre in Albi on Particulate Solids, the energy and Environment, UMR CNRS 5302, IMT Mines-Albi, France.

E-mail address: fabienne.espitalier@mines-albi.fr (F. Espitalier).

[7], an improvement of dermal and transdermal delivery [8] and offering a strategy for innovative cancers treatments or vaccines through functionalized nanoparticles leading to targeted therapies [9]. A common aspect of all cited area of application are the bioavailability improvement of the active and sides effect reduction. Considerable efforts are made to achieve the reproducible size and narrow distribution of the particles, which are decisive for the final efficiency. To produce these ultrafine nanoparticles with narrowed particle size distributions the choice of the composition and the generation process of SLN is therefore crucial. The most common method is the solvent injection method, which consists of injecting a water-miscible organic solution containing the lipid and surfactants into an aqueous medium through an injection needle [10]. On a pilot scale, the high-pressure homogenization process is the most widely used for reproducibility [11,12]. However, regardless of the generation method used, stability of SLN is limited. Indeed, a quick release of the active ingredient in aqueous media, due to a change in the polymorph of the solid lipid over time, is frequently reported [13].

To address this low stability, SADDs, like SLN, are commonly put in solid dosage form after the self-assembled process using spray-drying or freeze-drying processes [12,14,15]. These systems offer a longer storage due to the resulting solid formulation. They can be re-suspended upon request, and they may encapsulate drugs into nanoparticles for efficient and control delivery.

However, SADDs production is a multi-step process, and it could be highly valued in a single step process. Therefore, the development of solid SADDs (S-SADDs) through a one-step production process has been proposed with promising results using spray drying for self-assembled SLN [16]. The use of an energy-intensive drying process may make this alternative less attractive from the standpoint of research into more environmentally friendly production processes. Hence, green process, such as supercritical CO₂ processes (scCO₂) [17,18], could be explored.

scCO₂ processes have been used for the production of SLN in aqueous media [19], by antisolvent processes (Supercritical AntiSolvent (SAS), Supercritical Assisted Injection in a Liquid Antisolvent (SAILA)) [20,21], by Particle from Gas Saturated Solution (PGSS) [22] or by Rapid Expansion of Supercritical Solution (RESS) [23]. All these processes have advantages and disadvantages for SLN production. In the SAS process, an organic solution containing lipid(s) and active ingredient(s) is injected into a pressurized autoclave, scCO₂ acting as an antisolvent. Nevertheless, limited lipid supersaturations are generated for the crystallization due to their relatively low solubility in organic solvents and high solubility in scCO₂. This could lead in a significant loss of materials at the end of the process. More generally, lipids have high solubility in scCO₂ due to their non-polar nature as well as CO₂ [24]. Polar compounds, in turn, such as most pharmaceutical actives, are only slightly soluble in scCO₂ for the same reason [25]. RESS process, therefore, seems unsuitable for the vast majority of drugs since they must be dissolved in high quantities in scCO₂. However, RESS process is suitable for lipid crystallization, whereas SAS process is suitable for the crystallization of active ingredients [26,27]. Consequently, a new approach could be developed to process both RESS and SAS and thus, allowing the simultaneous co-crystallization of S-SADDs.

In the present work, a proof-of-concept study coupling RESS and SAS processes (RESS/SAS) was carried out using nifedipine (NIF) as drug model for the production of S-SADDs. Nifedipine (NIF) is a class II compound of the biopharmaceutical classification system (*i.e.* poorly water-soluble) [28]. A low oral bioavailability is associated to its low solubility and dissolution rate [29]. The development of NIF included in S-SADDs might overcome this issue. This study was conducted in three steps: (i) the development and adjustment of operating conditions to produce SLN suspension using solvent injection process, (ii) the optimization of the formulation to produce SLN with a mean particle size diameter close to 100 nm and stable at least 24 h, (iii) the transposition of the SLN formulation composition into the RESS/SAS coupled process for the production of S-SADDs.

2. Materials and methods

2.1. Materials

Nifedipine (dimethyl 2,6-dimethyl-4-(2-nitrophenyl)-1,4-dihydropyridine-3,5-dicarboxylate) (99.9 wt% purity, CAS: 21829-25-4) was purchased from LEAP Chem (China). Stearic acid (98 wt% purity, CAS: 57-11-4) was purchased from Alfa Aesar (USA). Polymers such as polyvinylpyrrolidone vinyl acetate (PVP-VA, CAS: 25086-89-9), polyvinylpyrrolidone K30 (PVP K30, CAS: 9003-39-8), poly(ethylene glycol)-*block*-poly(propylene glycol)-*block*-poly(ethylene glycol) (Poloxamer 188, CAS: 9003-11-6) and polyvinyl caprolactampolyvinyl acetate-polyethyleneglycol graft co-polymer (Soluplus®, CAS: 402932-23-4) were purchased from BASF (Germany). Phosphatidylcholine (PC, CAS: 8002-43-5) was purchased from Sigma Aldrich (France). Absolute ethanol (EtOH, CAS: 64-17-5) was purchased from VWR (France). UHPLC grade methanol and acetonitrile for HPLC analysis were purchased from Fischer Scientific (Illkirch, France). CO₂ (> 99.7% purity) was provided from Linde (France).

2.2. SLN formulation by solvent injection method and studied operating conditions

The experimental set-up consisted of using a jacketed reactor containing the dispersion solvent (purified water) under magnetic stirring (500 rpm) (Fig. 1, A). Two thermostatically controlled baths were used in order to set the operating temperature conditions. The first one was set for the injection temperature (Fig. 1, B), and the second one was a cooler to allow a rapid and reproducible cooling of the colloidal suspension (Fig. 1, C). SLN components were firstly dissolved in absolute ethanol using a stirred hotplate (70 °C). The resulting organic solution was then injected by the use of a syringe pump with controlled flow rate to evaluate the impact of injection rate (Fig. 1, D), through a needle (0.45 × 13 mm; Fig. 1, E), into the dispersion solvent (aqueous phase) at 45 °C or 70 °C. SLN suspension cooling temperatures at 3 °C and 25 °C (room temperature) were also evaluated. 3 mL of organic solution were injected into 150 mL of deionized water for optimization parameters assays. Variations of injection volumes were applied (from 1.17 mL (final lipid concentration = 0.5 mg/g) to 9.0 mL (final lipid concentration = 5 mg/g)) to minimize changes of lipid concentration in organic solution.

All formulations prepared by solvent injection method are presented in Table 1 and 2. The optimization of solvent process, Table 1, was achieved using a simple SLN formulation containing a solid lipid (stearic acid) and a polymeric surface stabilizer (PVP-VA). The investigation of the formulation composition, Table 2, was done by substituting or adding ingredients. PVP-VA was replaced by another polymeric surface stabilizer (PVP K30) or by amphiphilic copolymers (Poloxamer 188 or Soluplus®). The use of a co-surfactant agent (PC) was also investigated.

2.3. SLN characterization

2.3.1. Particle size, polydispersity index and zeta potential

Particle size, polydispersity index (PDI) and zeta potential were determined by Dynamic Light Scattering (DLS) using a Zetasizer Nano-ZS (Malvern Panalytical, UK). Particle size and PDI were measured using a 173° incident beam and zeta potential determination was done using folder capillary zeta cell. Before analysis, each sample was diluted in deionized water to reach a SLN suspension concentration of 1 mg.g⁻¹ to ensure that the light scattering intensity was within the instrument's sensitivity range. All measurements were carried out in triplicate at 20 °C and results were expressed as particle size average, PDI and zeta potential ± standard deviation (SD) of these 3 measurements.

2.3.2. Monitoring SLN stability upon storage

SLN were stored at 4 °C for one week and SLN z-average diameter,

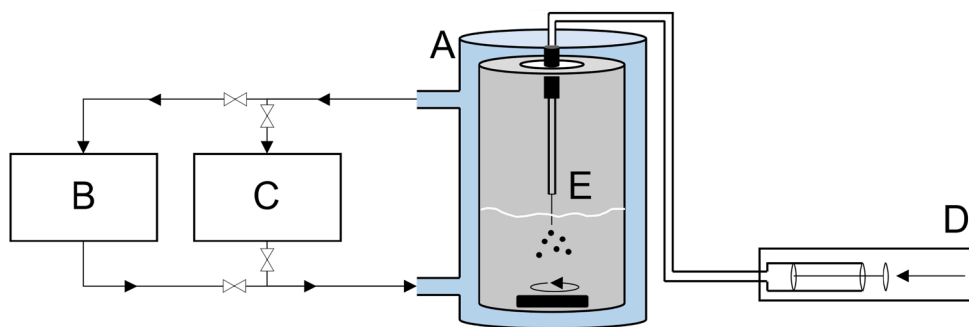


Fig. 1. Schematic representation of the solvent injection process. A, jacketed reactor; B, hot thermostatic bath; C, cold thermostatic bath; D, syringe pump; E, injection needle.

Table 1
Conditions applied for SLN suspension formulation and studied process parameters.

Process parameters	Injection rate (mL.min ⁻¹)			Stirring time after injection (min)				Aqueous phase temperature (°C)		Dispersion cooling temperature (°C)		Particle size (nm)	PDI	Zeta potential (mV)
	1	10	23	0	10	20	30	45	70	25	3			
F1	X				X			X		X		202.9 ± 7.0	0.169 ± 0.025	-29.0 ± 1.20
F2		X			X			X		X		185.1 ± 4.7	0.147 ± 0.023	-28.4 ± 1.69
F3			X		X			X		X		142.0 ± 3.8	0.173 ± 0.011	-27.1 ± 0.29
F4			X	X				X		X		288.8 ± 4.8	0.079 ± 0.027	-23.6 ± 1.65
F5			X		X			X		X		288.3 ± 6.9	0.078 ± 0.018	-20.3 ± 0.15
F6			X			X		X		X		348.8 ± 1.0	0.096 ± 0.024	-25.6 ± 0.82
F7			X				X	X		X		443.0 ± 3.4	0.155 ± 0.029	-24.3 ± 0.64
F8			X		X				X		X	156.3 ± 3.8	0.106 ± 0.009	-34.9 ± 2.26

Table 2
Composition of SLN suspensions for formulation screening.

Formulation	Components and concentration in SLN suspensions (mg.g ⁻¹)*						
	Stearic acid	PVPVA	Soluplus®	Poloxamer 188	PVP K30	Phosphatidylcholine	NIF
F9	0.5	1.0	-	-	-	-	-
F10	1.0	2.0	-	-	-	-	-
F11	1.5	3.0	-	-	-	-	-
F12	2.0	4.0	-	-	-	-	-
F13	5.0	10.0	-	-	-	-	-
F14	2.0	-	4.0	-	-	-	-
F15	2.0	-	-	4.0	-	-	-
F16	2.0	-	-	-	4.0	-	-
F17	2.0	-	-	-	4.0	1.0	-
F18	2.0	-	-	4.0	-	2.0	-
F19	2.0	-	-	4.0	-	2.0	0.2
F20	2.0	-	-	-	4.0	1.0	0.2

* Conditions used for the formulation of SLN suspension: stirring time after injection of 10 min, injection rate of 23 mL.min⁻¹, aqueous phase temperature at 70 °C and dispersion cooling temperature at 3 °C.

polydispersity index and zeta potential were measured immediately after preparation and also at 24 h and 48 h to follow nanoparticles stability over time. A low storage temperature was set to reduce stearic acid polymorphic changes [30].

2.3.3. Qualitative encapsulation efficiency

NIF qualitative encapsulation was conducted under optical microscopy. NIF SLN suspensions were observed through optical microscope (Leica® S9i) using polarized light to observe NIF expulsion over time. NIF SLN suspension were observed at 0 h, 24 h and 48 h. Images were acquired using Leica® KL300 LED camera.

2.4. S-SADDS production by scCO₂ RESS/SAS coupled processes

The crystallization apparatus process was purchased from Separex (France) (Fig. 2). In the first autoclave (Fig. 2, A), CO₂ was cooled in the liquid phase, pressurized over the critical pressure via a pump (Fig. 2, P)

and, heated above the critical temperature to obtain scCO₂ (Fig. 2, HE). RESS process comprises a thermostatically controlled dissolution autoclave able to achieve pressures up to 3 MPa (Fig. 2, B). The scCO₂ passed through this autoclave and dissolved stearic acid before reaching the atomization nozzle (Fig. 2, N) of the crystallization autoclave (Fig. 2, C). Simultaneously, an ethanolic solution containing the dissolved NIF, with or without additives (Fig. 2, D), was injected via an HPLC pump into the atomization nozzle (Fig. 2, N), which refers to the SAS process. The RESS/SAS coupled process was configured to mix components at the spray nozzle, as previously described in literature [31]. The antisolvent effect took place in the crystallization autoclave (Fig. 2, C), where the pressure was maintained above the critical pressure of the ethanol/scCO₂ mixture using a back pressure regulator (BPR). It ensures a single-phase fluid for the anti-solvent effect. During the process, to guarantee a significant supersaturation of the lipid and its crystallization, the pressure drop was around 7 MPa between the dissolution (B) and the crystallization autoclave (C).

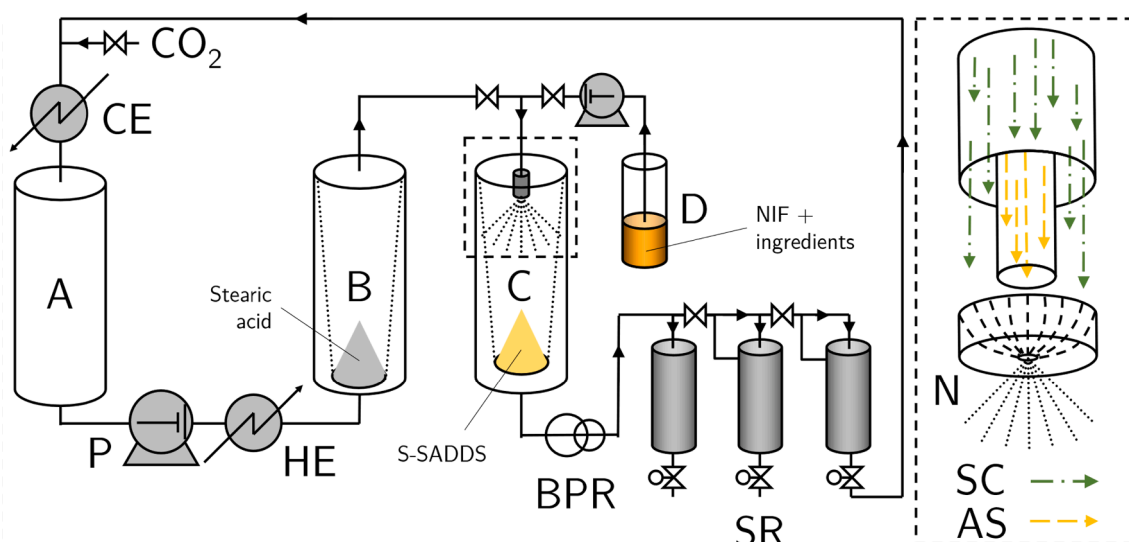


Fig. 2. Schematic representation of the coupled RESS/SAS process. A, liquid CO₂ reservoir; B, RESS dissolution vessel; C, crystallization vessel; D, solvent injection system; CE, cold exchanger; P, pump; HE, heat exchanger; BPR, back pressure regulator; SR, solvent recovery system; N, nozzle; SC, scCO₂ flux from B; AS, anti-solvent flux from D.

2.5. S-SADDS characterization

2.5.1. NIF assay

The concentration of NIF in the synthesized powders was quantified by high-pressure liquid chromatography (HPLC). Waters Acquity Arc (France) apparatus composed of a UV detector (2298 PDA detector) at 238 nm. A C18 column (Symmetry C18, 3.5 μm , 4.6 \times 75 mm) was used for the identification of NIF with a mobile phase composition of water/methanol/acetonitrile (50/45/5; v/v/v). The mobile phase flow rate was set at 0.7 mL.min⁻¹ with a NIF retention time of 10.3 min and an injection volume of 5 μL . Samples were dissolved in methanol prior the analysis and quantified using a NIF calibration curve in this same solvent.

2.5.2. X-Ray powder diffraction analysis (XRPD)

XRPD analysis of the processed and commercial drug powders was performed using X' PERT PRO MDP, Philips PANalytical (USA) apparatus with CuK α radiation. Powders were stack into a sample holder and diffractogram patterns were obtained at 45 kV, 40 mA at 2 θ in a range of 5-50° using a scanning rate of 1.228 min⁻¹.

2.5.3. Differential Scanning calorimetry analysis (DSC)

Differential Scanning Calorimetry (DSC) analysis of commercial NIF and processed samples was performed using a DSC Q200 (TA Instrument, USA). Samples were placed in a non-hermetically closed aluminum pan. The analysis was carried out in a temperature range of 20 to 210 °C (293.15 to 483.15 K) at a heating rate of 5 °C.min⁻¹ under a dry nitrogen flow rate of 50 mL.min⁻¹.

2.5.4. Fourier transform Infra-Red spectrometry (FTIR)

FTIR spectra were acquired using a Nicolet iS50 spectrometer (Thermo Scientific, France) apparatus in Attenuated Total Reflectance (ATR) mode. Samples were recorded between 4000 and 400 cm⁻¹ with a spectral resolution of 4 cm⁻¹.

2.5.5. Scanning electron microscopy (SEM)

Scanning electron microscope (MT-3000, Hitachi, Tokyo, Japan) was used to observe the morphological shape of processed materials. Before analysis, samples were fixed on a SEM stub through a double-sided adhesive tape and finally plated with platinum for 100 s at 2 kV.

3. Results and discussion

3.1. SLN dispersion obtained by solvent injection method

The development of SLN suspension was performed in two different steps. In the first one, the impact of solvent injection process parameters was investigated with a simple formulation (without NIF) to choose the suitable settings and achieve low particles size, low PDI and high zeta potential. In the second step, SLN formulation screening was conducted by evaluating the influence of the lipid concentration, polymer type and the addition of a co-surfactant, with or without NIF, using selected process parameters. The best SLN composition that allows suitable physicochemical properties was selected for RESS/SAS transposition.

3.1.1. Influence of operating parameters

Formulations were prepared in two blocks according to the tested parameter: i) injection rate (Table 1, F1 to F3); ii) stirring time after injection, aqueous phase temperature and dispersion cooling temperature impact (Table 1, F4 to F8). Results showed that a rapid injection rate (23 mL.min⁻¹) leads to smaller SLN size (142.0 \pm 3.8 nm) compared to a lower injection rate. A stirring time after injection above 10 min seems to increase particle size (from \sim 288 nm at 10 min to \sim 443 nm at 30 min) and PDI (from \sim 0.078 at 10 min to \sim 0.155 at 30 min). Using the best previous conditions (10 min and 23 mL.min⁻¹), a combined high aqueous dispersion temperature at 70 °C and rapid dispersion cooling temperature at 3 °C after injection yields the best results (SLN particle size of 156.3 nm \pm 3.8, PDI of 0.106 \pm 0.009 and zeta potential of -34.9 mV), compared to aqueous phase temperature at 45 °C and dispersion cooling temperature at 25 °C (See F5 and F8, Table 1). The formation of SLNs occurs when stearic acid crystallizes due to high supersaturation generated by antisolvent effect combined with temperature effect [32]. Cooling the aqueous phase at 3 °C favors a more rapid crystallization of stearic acid compared to cooling aqueous phase at 25 °C. Based on these results, an injection rate of 23 mL.min⁻¹, a stirring time after injection of 10 min and a dispersion cooling temperature of 3 °C were set as process parameters for the evaluation of SLN composition (Table 2).

3.1.2. Formulation screening and SLN storage stability

According to Fig. 3, a slight decrease of the size was observed through an increase concentration of stearic acid and PVP-VA (Table 2, F9-F13). However, at a final concentration of 5 mg.g⁻¹ stearic acid and

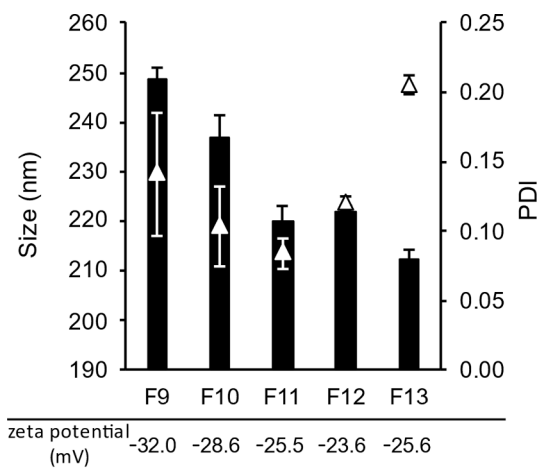


Fig. 3. Particle size average, PDI and zeta potential of formulations F9 to F13 containing stearic acid and PVP-VA at increasing concentration (from respectively 0.5:1 to 5:10). Bar graphs represent the size and triangles the PDI. Error bars = SD.

10 mg.g⁻¹ PVP-VA (F13), a phase separation occurs, characterized by a creaming phenomenon. Taking into account these results, final concentrations of 2 mg.g⁻¹ lipid and 4 mg.g⁻¹ of polymer were selected for the next step. This choice was justified because any physical instability was observed in this SLN suspension which presented particle size of 222.0 ± 1.0 nm, a PDI of 0.120 ± 0.005 and a zeta potential of -23.6 mV at generation. In addition, higher lipid concentration allows a higher amount of encapsulated drug.

The impact of polymer type was examined by replacing the PVP-VA with PVP K30, Poloxamer188 or Soluplus® to reduce the size of SLN suspension (Table 2). The formulation obtained with Soluplus® exhibited larger particle sizes than those obtained with PVP-VA (Fig. 4, a, F14). Using Poloxamer188, SLN particle size was the smallest obtained, despite low stability over time (Fig. 4, a, F15). In contrast, PVP K30 allowed lower particle size average and demonstrated a high ability to maintain the SLN particle size for 48 h (Fig. 4, a, F16). Besides, PVP K30 allowed less viscous aqueous phase, which improved the formulation dispersion ability. PVP K30 and Poloxamer 188 were the two polymers retained in the SLN suspension composition.

To further reduce SLN size, phosphatidylcholine (PC) was added as a co-surfactant to the formulation. As shown in the Fig. 4 (F17 and F18), the presence of PC induced an important reduction in SLN particle size, an increased PDI and a decrease of zeta potential from -30 up to -40 mV (Fig. 4, b). Thus, SLN suspension containing PC resulted in a particle size average under 100 nm. Moreover, a sufficient 24 h stable SLN suspension was obtained as SADDs are used as an on-demand drug delivery. It is important to highlight that the addition of NIF in placebo formulation did not change the particle size average, PDI and zeta potential (Fig. 4, a and b, F19-F20).

3.1.3. SLN qualitative encapsulation efficiency

A qualitative evaluation of the NIF encapsulation efficiency (EE) was determined. Visual NIF expulsion phenomenon from lipid matrix over time, was evaluated. Fig. 5 illustrates the microscopic images obtained from the F19 and F20, immediately after SLN formation, and then at 24 h and 48 h. The formulation containing Poloxamer 188 presented bright yellow spikes since production (Fig. 5, F19). These yellow spikes correspond to NIF crystals expelled from SLN, which are growing over time. Using PVP-K30, no yellow spikes were observed up to 24 h by optical microscopy (Fig. 5, F20). However, agglomerated NIF crystals characterized by yellow spots were observed at 48 h. From literature, a rapid release of active ingredients is regularly described from SLN, followed by a prolonged release [33]. This rapid release of the active ingredient can be restrictive for storage and seems to be observed in the qualitative release of formulations F19 and F20. As optical microscopy images of F20 showed a reduced release of NIF compared to F19, this formulation containing PVP-30 was chosen for further S-SADDs production using scCO₂ technology. Furthermore, the RESS/SAS process needs to maintain crystallization autoclave temperature (Fig. 2, C) close to the melting point of Poloxamer 188 (52 °C), which could be a limitation linked to powder crystallization.

3.2. Production of S-SADDs by scCO₂ assisted processes

Once the formulation parameters achieved to obtain a stable formulation for at least 24 h with a particle size below 100 nm, coupled RESS/SAS processes were designed. Owing to the high quantities of stearic acid required in the final formulations and their low solubility in ethanol, it was necessary to crystallize them via the RESS process. Conversely, the other ingredients (PVP K30, PC and NIF) are poorly soluble in scCO₂, which allows their crystallization using SAS process.

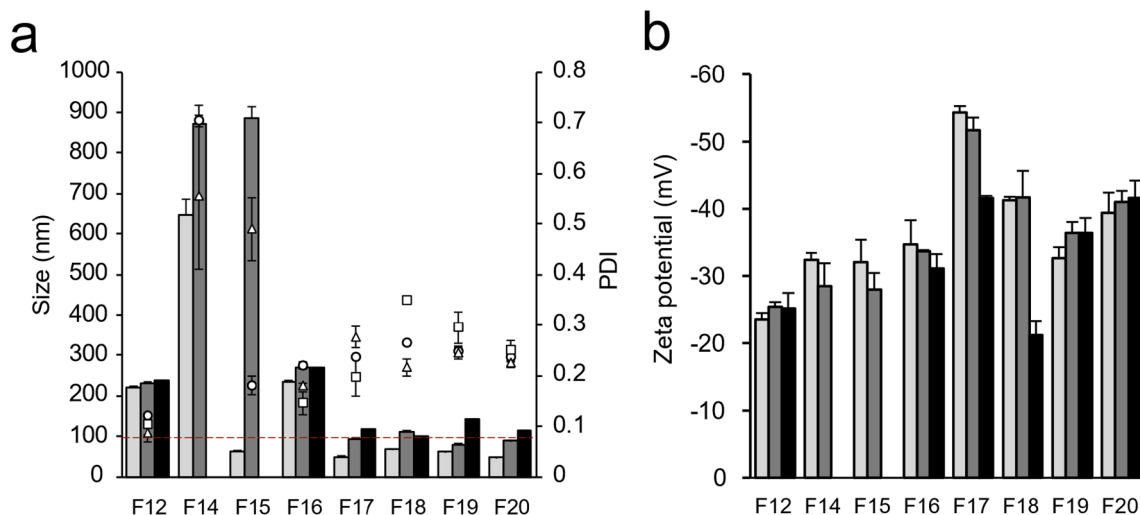


Fig. 4. Particle size, PDI and zeta potential (b) of formulations 12 to 20 at 0 h, 24 h and 48 h after the solvent injection process. Bar graphs represent the average particle size and zeta potential of three measurements at 0 h (light gray), 24 h (gray), 48 h (dark). PDI is represented as dots on right y axis (0 h), triangle (24 h) and square (48 h). Errors bars = SD, SA = stearic acid. F14 = SA + Soluplus®, F15 = SA + Poloxamer 188, F16 = SA + PVPK30; F17 = F16 + PC; F18 = F15 + PC; F19 = F18 + NIF; F20 = F17 + NIF.

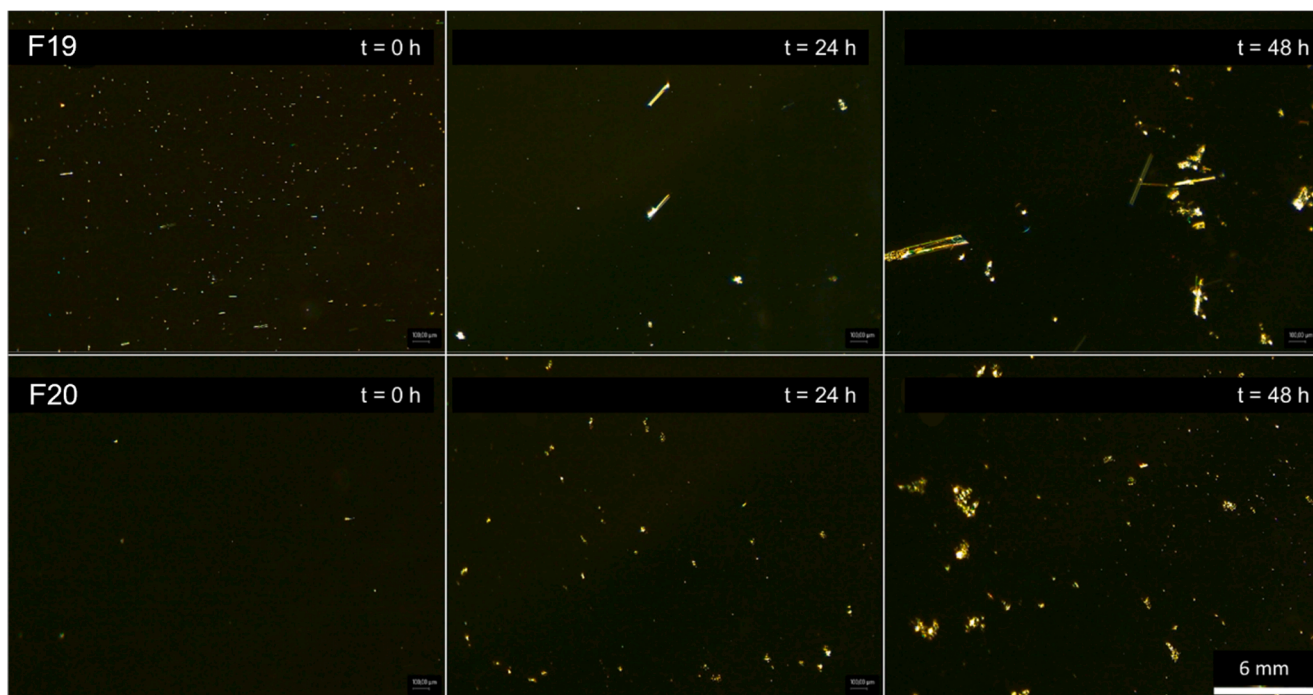


Fig. 5. SLN dispersion under optical microscope with polarized light at 0 h, 24 h and 48 h.

Thus, a co-injection of a scCO_2 -stearic acid mixture in RESS and an ethanolic solution containing the other ingredients in SAS was performed for their simultaneous co-crystallization.

3.2.1. Operating parameters for crystallization by supercritical CO_2 process

A stepwise experimental plan was developed to adjust parameters of RESS/SAS processes for S-SADDS generation (Table 3). For that, NIF crystallization by SAS process was first carried out to define pressure and temperature operating conditions to obtain high-rate efficiency. Based on this preliminary study, coupled RESS/SAS processes experiments were performed to produce S-SADDS. The operating conditions for SAS process were set in order to have 2% ($w_{\text{EtOH}}/w_{\text{CO}_2}$) of EtOH injected into the crystallization autoclave (Table 3, F21). In order to ensure process feasibility, dissolved NIF in ethanol at a concentration of $52 \text{ mg}\cdot\text{g}^{-1}$ at 60°C (experimental equilibrium concentration $55.5 \text{ mg}\cdot\text{g}^{-1}$ at 45°C , data not shown) was atomized through a 0.3 mm diameter nozzle. The

Table 3
Studied operating parameters for SAS and coupled RESS/SAS processes.

Formulation	SAS process	Coupled RESS/SAS processes			
	F21	F22	F23	F24	F25
Theoretical NIF (wt. %)	100.0	9.0	9.0	6.3	5.9
Stearic acid (wt. %)	/	89.0	89.0	62.3	58.8
PC (wt. %)	/	/	/	31.4	29.4
PVP K30 (wt. %)	/	/	/	/	5.9
EtOH- CO_2 ratio (%)	2.00	3.96	0.36	0.36	0.36
CO_2 flux (kg/h)	10.0	8.5	15.9	16.0	15.0
EtOH flux (kg/h)	0.20	0.31	0.06	0.06	0.06
CNIF ($\text{mg}/\text{g}_{\text{EtOH}}$)	52.20	56.37	56.03	58.77	55.51
NIF injected (g)	1.00	1.03	0.51	1.07	1.01
B vessel (MPa; $^\circ\text{C}$)	/	16.5; 65	16.0; 62	14.5; 62	14.2; 61
C vessel (MPa; $^\circ\text{C}$)	12.3; 44	7.7; 35	9.8; 39	7.9; 37	10.1; 39
Extracted stearic acid (g)	/	2.16	8.05	6.37	10.42
Crystallized weight (g)	0.98	3.09	6.93	7.7	13.52
Measured NIF (wt. %)	98.10	39.5	4.4	5.8	5.6

pressure inside the crystallization vessel was maintained above the critical point of the $\text{scCO}_2/\text{EtOH}$ at 2% (over 9 MPa). This step was able to ensure a high yield efficiency of 98.1 % by SAS process (Table 3, F21-SAS process).

The coupled RESS/SAS processes for co-crystallization of stearic acid and NIF was then performed first with the desired ratio of 9 % ($w_{\text{NIF}}/w_{\text{solid}}$) (Table 3, F22). Crystallization through the RESS process consists by dissolving raw stearic acid in a dedicated autoclave under high pressure and temperature (Fig. 2, B). The scCO_2 passing through the autoclave dissolves the compound. This stearic acid/ CO_2 mixture is then expanded in another autoclave (Fig. 2, C), inducing supersaturation and crystallization of stearic acid. The pressure and temperature in the crystallization autoclave were previously set from SAS process (F21). Operating conditions of dissolution autoclave must then be determined for the RESS process. To determine RESS operating parameters, equilibrium solubilities in scCO_2 of stearic acid were extracted from literature [24,34]. scCO_2 flow rate was set considering not only mass fraction extraction of stearic acid at the exit of the cell (Fig. 2, B) but also the amount of non-crystallizable mass fraction in the crystallization autoclave (Fig. 2, C) due to a high pressure and co-solvent mixture (Eq.1). The extraction rate, temperatures, and pressures were determined to theoretically and simultaneously crystallize at the desired ratio (Table 3, F22).

$$\frac{\dot{w}_{\text{SAC}}}{\dot{w}_{\text{NIFC}}} = \frac{\dot{w}_{\text{SAE}(T,P)} - \dot{w}_{\text{SANC}(T,P;\% \text{EtOH})}}{\dot{w}_{\text{NIF}_1} - \dot{w}_{\text{NIFNC}(T,P;\% \text{EtOH})}} = 10\# \quad (1)$$

where \dot{w}_{SAC} corresponds to the crystallization mass flow of stearic acid, \dot{w}_{NIFC} the crystallization mass flow of NIF, $\dot{w}_{\text{SAE}(T,P)}$ the extraction mass flow in the B vessel, $\dot{w}_{\text{SANC}(T,P;\% \text{EtOH})}$ the non-crystallizable mass flow of stearic acid in the C vessel, \dot{w}_{NIF_1} the injection mass flow of NIF and $\dot{w}_{\text{NIFNC}(T,P;\% \text{EtOH})}$ the non-crystallizable mass flow NIF in the C vessel (estimated zero from NIF-SAS experiment).

The percentage of EtOH- CO_2 in the crystallization vessel was finally set at 3.96%. An increased EtOH percentage in the final mixture was fixed, compared to F21, with the risk of slightly reduced NIF crystallization yield. Conversely, the pressure of the crystallization autoclave was set lower in order to maximize the supersaturation of stearic acid

and improve the yield of NIF. This first RESS/SAS experiment resulted in a powder composed of 39.4 %wt of NIF while the theoretical percent of NIF should be 9.0 %wt. This finding can probably be assigned to the non-saturation of stearic acid in scCO₂ at the exit of the dissolution vessel (Fig. 2, B). To correct the desired ratios, extracted mass fraction of stearic acid in scCO₂ was calculated from F22 to adjust injection rates of scCO₂ and EtOH (Eq.2).

$$w_{Stearicacid} = \frac{W_{extractedStearicacid}}{(Qw_{CO_2} \times t_{exp}) + W_{extractedStearicacid}} \quad \#\# \quad (2)$$

Where $w_{stearicacid}$ correspond to the mass fraction equilibrium of stearic acid in scCO₂ at defined temperature and pressure, Qw_{CO_2} correspond to the flow rate of CO₂ expressed in kg.h⁻¹ and t_{exp} the time of experiment in hours.

From the adjustment, the new 0.36% EtOH-CO₂ ratio was fixed to theoretically crystallized NIF and stearic acid at the desire ratio. The

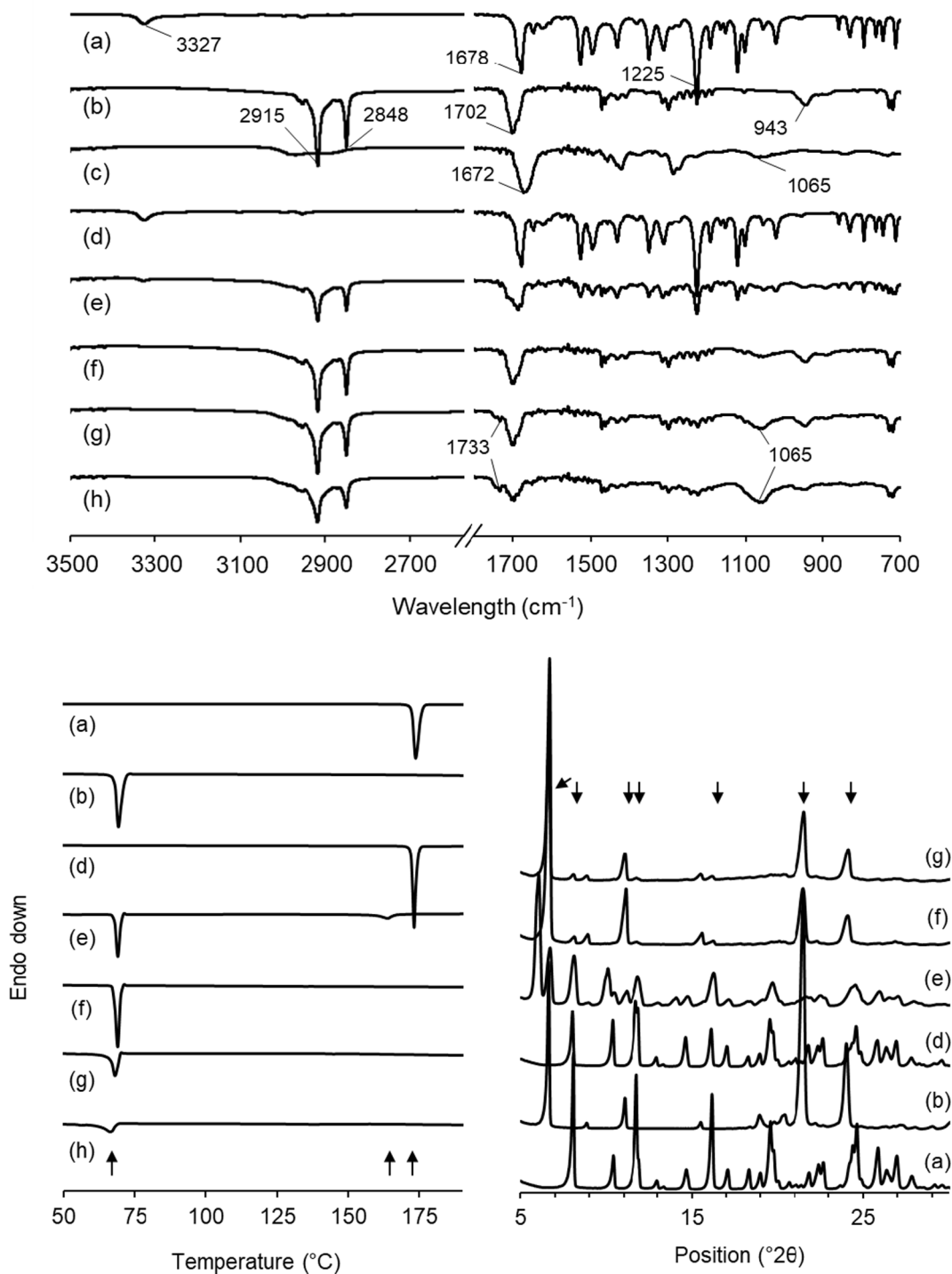


Fig. 6. Powder characterizations of unprocessed and processed samples from FTIR (top), DSC (left) and XRPD (right) analysis. Letters correspond to: (a) Raw NIF, (b) Raw stearic acid, (c) PVP K30, (d) F21 (NIF-SAS process), (e) F22 (NIF/Stearic acid), (f) F23 (NIF/Stearic acid_2), (g) F24 (NIF/Stearic acid/PC), (h) F25 (NIF/Stearic acid/PC/PVP K30). Arrows represent significative peaks of NIF and stearic acid.

modification of operating conditions resulting to a closer ratio between NIF and stearic acid with 4.4%wt of NIF (9.0%wt theoretically) in the resulting S-SADDS (Table 3, F23). These defined operating conditions were kept for F24 and F25 production. Similar result was obtained in presence of PC in the injected organic solution (F24). The entire SLN optimized formulation was crystallized with adjusted parameters to finally produce S-SADDS containing 5.6%wt of NIF (5.9%wt theoretically) (F25).

3.2.2. Powder characterizations and morphological evaluation

In order to verify the presence of all the components introduced in the process, DSC, XRPD and FTIR characterization methods were carried out (Fig. 6). Physicochemical characterizations of processed raw NIF using SAS process (F21) showed specific vibration bands identified at 1225 cm^{-1} (C–O stretch), 1678 cm^{-1} (C = O stretch) and 3327 cm^{-1} (N–H stretch) (Fig. 6, a and d). DSC thermogram highlighted melting points of $171\text{ }^{\circ}\text{C}$ for raw and processed NIF suggesting the same polymorphic structure of both compounds (Fig. 6, a and d). According to XRPD analysis, NIF exhibited its most stable form, polymorph A, as most intense peaks were found at 2θ degree of 8.1° , 11.7° and 16.2° [35].

Analysis of F22 from RESS/SAS process showed the presence of NIF and stearic acid (Fig. 6, e). FTIR spectra from this sample showed specific bands of stearic acid at 943 cm^{-1} (–OH bend from carboxylic acid), 1702 cm^{-1} (C = O stretch) and $2848/2915\text{ cm}^{-1}$ (C–H stretch). The crystallinity of F22 was confirmed through DSC thermograms which highlighted the melting point of stearic acid at $69\text{ }^{\circ}\text{C}$, similar to raw stearic acid (Fig. 6, b and e), and the melting point of NIF at $163\text{ }^{\circ}\text{C}$. The reduction of NIF melting point could correspond to the specific polymorph B [35] or the formation of an eutectic mixture between NIF and stearic acid. Interestingly, stearic acid XRPD analysis showed a mixture of polymorphic forms C and B which are characterized by most intense Bragg peaks at 5.7° and 6.6° 2θ degree, respectively (Fig. 6, a, b and e) [36].

Fitting ratios to produced F23 showed in XRPD analysis the presence of commercial stearic acid polymorph after crystallization (Fig. 6, b and f). This result suggests that polymorphic control of stearic acid could be achieved by varying operating crystallization conditions of coupled RESS/SAS processes. Intensity reduction of NIF characteristic Bragg peaks was observed maybe due to the reduced percentage in the formulation. Moreover, FTIR and DSC analysis were not enough

sensitive to detect the presence of NIF.

The addition of PC to crystallized F24 made the powder characterization more difficult. Conforming to sample analysis no stearic acid polymorphic change was observed. In contrast, it was difficult to distinguish PC from FTIR, XRPD or DSC analysis (Fig. 6, f). Two specific bands of PC seem to appear in FTIR analysis at 1065 cm^{-1} , which could correspond to inorganic phosphate vibration [37], and at 1733 cm^{-1} (C = O stretch). These findings could not be confirmed using XRPD or DSC analysis as PC is not a crystalline compound.

Similar difficulties were observed for the formulation analysis containing PVP K30 (Table 3, F25). FTIR analysis could not specifically identify PVP K30 or PC because theoretical vibrations of these two molecules were too closed. However, F25 DSC analysis suggested an evaporation endotherm around $70\text{ }^{\circ}\text{C}$ due to naturally present moisture (Fig. 6, h), as previously described for formulation containing PVP K30 [38]. For this kind of innovate system, specific characterization methods should be developed for each S-SADDS compound to determine their exact concentration and to identify drug or excipient potential polymorphs.

Morphologies of self-assembled powders, obtained by SEM images were homogeneous (Fig. 7). A characteristic plate-like crystallization of stearic acid was observed [36]. The use of other lipids, usually used for SLN production, or even other solvents could change this morphology [20]. No traces of NIF crystals classically produced by SAS process were observed, while their presence was previously confirmed through characterization studies. SEM images of S-SADDS F23, F24 and F25 showed a similar powder facies, however, F24 and F25 appeared to have a waxier appearance similar to PC texture. Although, generated solids were composed of agglomerated plate-like crystals. Redispersion of this type of agglomerated particles may need energy input. Preliminary redispersion study of F24 were easily achieved by the use of ultrasounds (13 W, 10 min) with the obtention of two distribution particle size of 52.2 nm (33% v/v) and 732.4 nm (66% v/v) (data not shown). Distribution of the large particles could be assigned to particle agglomeration as previously described in literature [16]. The production of different morphological shape may limit the formation of agglomerates. Various morphological solid production have been already demonstrated using the SAS process [21,39,40]. Mechanisms controlling the morphology of powders from SAS process were also modeled and validated [41–43]. Process parameters for the coupled RESS/SAS processes could therefore

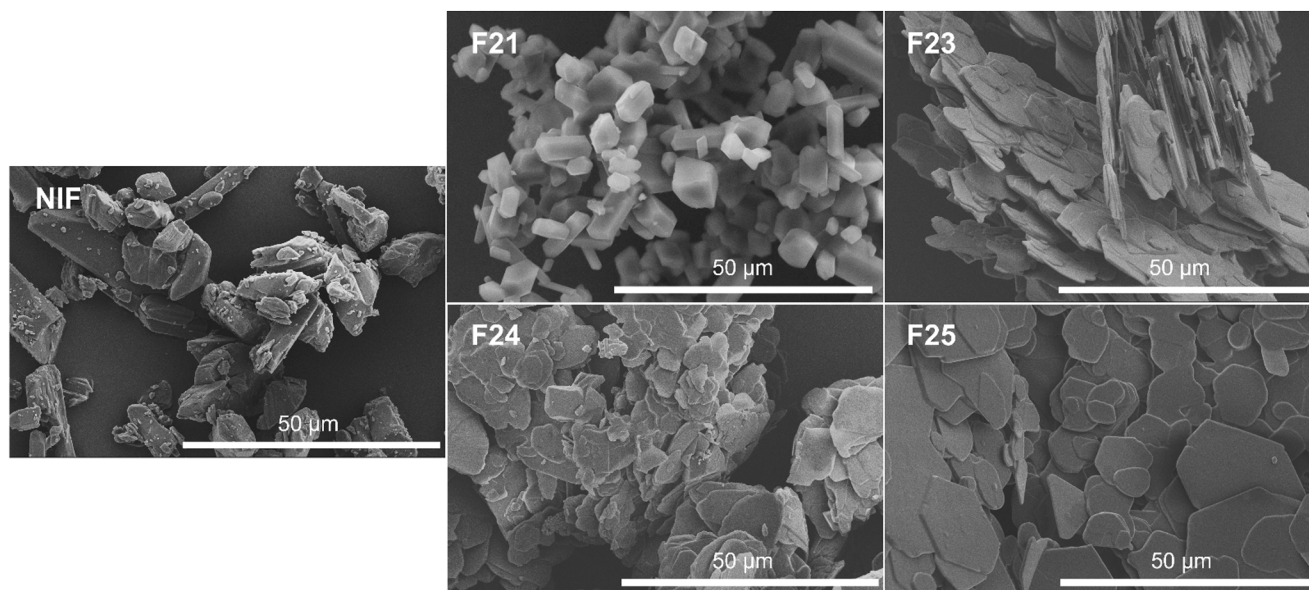


Fig. 7. Scanning electron microscopy of obtained processed samples from RESS/SAS (F23, F24 and F25) compared to raw NIF and NIF/SAS (F21). Scale bar = $50\text{ }\mu\text{m}$; magnification: $\times 1\ 500$.

be optimized to generate particles with lower agglomeration properties for an effective S-SADDS re-suspension.

4. Conclusion

Proof-of-concept development of S-SADDS from the innovative coupled RESS/SAS process was designed to provide one-step on-demand drug delivery system. Preliminary optimization of solvent injection process and formulation of SLN was achieved, which allowed the production of particle size close to 100 nm up to 24 h after the production. The SLN formulation had been successfully transposed into the eco-friendly RESS/SAS scCO₂-assisted process, allowing a simultaneous crystallization of solid self-assembled formulation in a one step process. The continuous high yield production RESS/SAS process demonstrates a great potential to generate complex solid with high control of operating conditions. Finally, RESS/SAS process innovation seems to be very promising for the generation of complex solids, intermediate products or for the development of innovative S-SADDS.

CRedit authorship contribution statement

Thibault Massias: Conceptualization, Methodology, Investigation, Formal analysis, Writing – original draft. **Suénia de Paiva Lacerda:** Conceptualization, Validation, Writing – review & editing. **Jacqueline Resende de Azevedo:** Validation, Writing – review & editing. **Jean-Jacques Letourneau:** Methodology, Validation. **Philomène Dos Santos:** Methodology, Investigation, Formal analysis. **Marie-Alexandrine Bolzinger:** Validation, Supervision. **Fabienne Espitalier:** Validation, Supervision.

Declaration of Competing Interest

The authors declare that they have no known competing financial interests or personal relationships that could have appeared to influence the work reported in this paper.

Data availability

Data will be made available on request.

Acknowledgements

The authors acknowledge the support of the French Ministère de l'Enseignement Supérieur et de la Recherche and the Ministère de l'Industrie.

References

- [1] J. Shi, Z. Xiao, N. Kamaly, O.C. Farokhzad, Self-assembled targeted nanoparticles: Evolution of technologies and bench to bedside translation, *Acc. Chem. Res.* 44 (2011) 1123–1134, <https://doi.org/10.1021/ar200054n>.
- [2] L.T. Varma, N. Singh, B. Gorain, H. Choudhury, M.M. Tambuwala, P. Kesharwani, R. Shukla, Recent Advances in Self-Assembled Nanoparticles for Drug Delivery, *Curr. Drug Deliv.* 17 (2020) 279–291, <https://doi.org/10.2174/1567201817666200210122340>.
- [3] W. Mehnert, K. Mäder, Solid lipid nanoparticles: Production, characterization and applications, *Adv. Drug Deliv. Rev.* 47 (2001) 165–196, [https://doi.org/10.1016/S0169-409X\(01\)00105-3](https://doi.org/10.1016/S0169-409X(01)00105-3).
- [4] M.C. García, C. Aloisio, R. Onnainty, G. Ullio-Gamboa, Self-assembled nanomaterials, in: *Nanobiomaterials Nanostructured Mater.* Biomed, Appl., Woodhead Publishing, 2018, pp. 41–94, <https://doi.org/10.1016/B978-0-08-100716-7.00003-9>.
- [5] M.A. Bolzinger, S. Briançon, J. Pelletier, Y. Chevalier, Penetration of drugs through skin, a complex rate-controlling membrane, *Curr. Opin. Colloid Interface Sci.* 17 (2012) 156–165, <https://doi.org/10.1016/j.cocis.2012.02.001>.
- [6] M.J. Mitchell, M.M. Billingsley, R.M. Haley, M.E. Wechsler, N.A. Peppas, R. Langer, Engineering precision nanoparticles for drug delivery, *Nat. Rev. Drug Discov.* 20 (2021) 101–124, <https://doi.org/10.1038/s41573-020-0090-8>.
- [7] A.R. Neves, J.F. Queiroz, S.A. Costa Lima, F. Figueiredo, R. Fernandes, S. Reis, Cellular uptake and transcytosis of lipid-based nanoparticles across the intestinal barrier: Relevance for oral drug delivery, *J. Colloid Interface Sci.* 463 (2016) 258–265, <https://doi.org/10.1016/j.jcis.2015.10.057>.
- [8] M. Sala, R. Diab, A. Elaissari, H. Fessi, Lipid nanocarriers as skin drug delivery systems: Properties, mechanisms of skin interactions and medical applications, *Int. J. Pharm.* 535 (2018) 1–17, <https://doi.org/10.1016/j.ijpharm.2017.10.046>.
- [9] T.T.H. Thi, E.J.A. Suys, J.S. Lee, D.H. Nguyen, K.D. Park, N.P. Truong, Lipid-based nanoparticles in the clinic and clinical trials: From cancer nanomedicine to COVID-19 vaccines, *Vaccines*. 9 (2021) 1–29, <https://doi.org/10.3390/vaccines9040359>.
- [10] M.A. Schubert, C.C. Müller-Goymann, Solvent injection as a new approach for manufacturing lipid nanoparticles - Evaluation of the method and process parameters, *Eur. J. Pharm. Biopharm.* 55 (2003) 125–131, [https://doi.org/10.1016/S0939-6411\(02\)00130-3](https://doi.org/10.1016/S0939-6411(02)00130-3).
- [11] C. Dumont, V. Jannin, C. Miolane, Q. Lelong, J.P. Valour, S. Urbaniak, H. Fessi, S. Bourgeois, A proof-of-concept for developing oral lipidized peptide Nanostructured Lipid Carrier formulations, *J. Drug Deliv. Sci. Technol.* 54 (2019), 101394, <https://doi.org/10.1016/j.jddst.2019.101394>.
- [12] H. Ohshima, A. Miyagishima, T. Kurita, Y. Makino, Y. Iwao, T. Sonobe, S. Itai, Freeze-dried nifedipine-lipid nanoparticles with long-term nano-dispersion stability after reconstitution, *Int. J. Pharm.* 377 (2009) 180–184, <https://doi.org/10.1016/j.ijpharm.2009.05.004>.
- [13] C. Freitas, R.H. Müller, Correlation between long-term stability of solid lipid nanoparticles (SLN(TM)) and crystallinity of the lipid phase, *Eur. J. Pharm. Biopharm.* 47 (1999) 125–132, [https://doi.org/10.1016/S0939-6411\(98\)00074-5](https://doi.org/10.1016/S0939-6411(98)00074-5).
- [14] T. Yi, J. Wan, H. Xu, X. Yang, A new solid self-microemulsifying formulation prepared by spray-drying to improve the oral bioavailability of poorly water soluble drugs, *Eur. J. Pharm. Biopharm.* 70 (2008) 439–444, <https://doi.org/10.1016/j.ejpb.2008.05.001>.
- [15] K. Cerpnjak, A. Zvonar, F. Vrečer, M. Gašperlin, Development of a solid self-microemulsifying drug delivery system (SMEDDS) for solubility enhancement of naproxen, *Drug Dev. Ind. Pharm.* 41 (2015) 1548–1557, <https://doi.org/10.3109/03639045.2014.971031>.
- [16] B. Sanchez-Vazquez, J.B. Lee, M. Strimaite, A. Buanz, R. Bailey, P. Gershkovich, G. Pasparakis, G.R. Williams, Solid lipid nanoparticles self-assembled from spray dried microparticles, *Int. J. Pharm.* 572 (2019), 118784, <https://doi.org/10.1016/j.ijpharm.2019.118784>.
- [17] J. Fages, H. Lochard, J.J. Letourneau, M. Saucieu, E. Rodier, Particle generation for pharmaceutical applications using supercritical fluid technology, *Powder Technol.* 141 (2004) 219–226, <https://doi.org/10.1016/j.powtec.2004.02.007>.
- [18] P. Chakravarty, A. Famili, K. Nagapudi, M.A. Al-Sayah, Using supercritical fluid technology as a green alternative during the preparation of drug delivery systems, 2019, <https://doi.org/10.3390/pharmaceutics11120629>.
- [19] F. Corrias, F. Lai, New Methods for Lipid Nanoparticles Preparation, *Recent Pat. Drug Deliv. Formul.* 5 (2011) 201–213, <https://doi.org/10.2174/187221111797200597>.
- [20] P. Trucillo, R. Campardelli, Production of solid lipid nanoparticles with a supercritical fluid assisted process, *J. Supercrit. Fluids*. 143 (2019) 16–23, <https://doi.org/10.1016/j.supflu.2018.08.001>.
- [21] L. Lesoin, C. Crampon, O. Boutin, E. Badens, Preparation of liposomes using the supercritical anti-solvent (SAS) process and comparison with a conventional method, *J. Supercrit. Fluids*. 57 (2011) 162–174, <https://doi.org/10.1016/j.supflu.2011.01.006>.
- [22] O.N. Ciftci, F. Temelli, Formation of solid lipid microparticles from fully hydrogenated canola oil using supercritical carbon dioxide, *J. Food Eng.* 178 (2016) 137–144, <https://doi.org/10.1016/j.jfoodeng.2016.01.014>.
- [23] Z. Akbari, M. Amanlou, J. Karimi-Sabet, A. Golestani, M.S. Niassar, Production of ibuprofen-loaded solid lipid nanoparticles using rapid expansion of supercritical solution, *J. Nano Res.* 31 (2015) 15–29, <https://doi.org/10.4028/www.scientific.net/JNanoR.31.15>.
- [24] P. Maheshwari, Z.L. Nikolov, T.M. White, R. Hartel, Solubility of fatty acids in supercritical carbon dioxide, *J. Am. Oil Chem. Soc.* 69 (1992) 1069–1076, <https://doi.org/10.1007/BF02541039>.
- [25] M. Baghbanbashi, N. Hadidi, G. Pazuki, Solubility of pharmaceutical compounds in supercritical carbon dioxide: Application, experimental, and mathematical modeling, in: *Green Sustain. Process Chem. Environ. Eng. Sci. Supercrit. Carbon Dioxide as Green Solvent*, Elsevier, 2019, pp. 185–254, <https://doi.org/10.1016/B978-0-12-817388-6.00010-6>.
- [26] M.S. Kim, S. Lee, J.S. Park, J.S. Woo, S.J. Hwang, Micronization of cilostazol using supercritical antisolvent (SAS) process: Effect of process parameters, *Powder Technol.* 177 (2007) 64–70, <https://doi.org/10.1016/j.powtec.2007.02.029>.
- [27] A. Montes, M.D. Gordillo, C. Pereyra, E.J. Martínez De La Ossa, Polymer and ampicillin co-precipitation by supercritical antisolvent process, *J. Supercrit. Fluids*. 63 (2012) 92–98, <https://doi.org/10.1016/j.supflu.2012.01.001>.
- [28] G.L. Amidon, H. Lennernäs, V.P. Shah, J.R. Crison, A Theoretical Basis for a Biopharmaceutical Drug Classification: The Correlation of In Vitro Drug Product Dissolution and in Vivo Bioavailability, *Pharm. Res. An Off. J. Am. Assoc. Pharm. Sci.* 12 (1995) 413–420, <https://doi.org/10.1023/A:1016212804288>.
- [29] T.S. Foster, S.R. Hamann, V.R. Richards, P.J. Bryant, D.A. Graves, R.G. McAllister, Nifedipine Kinetics and Bioavailability After Single Intravenous and Oral Doses in Normal Subjects, *J. Clin. Pharmacol.* 23 (1983) 161–170, <https://doi.org/10.1002/j.1552-4604.1983.tb02720.x>.
- [30] R.-A. Hernández-Esquível, G. Navarro-Tovar, E. Zárate-Hernández, P. Aguirre-Bañuelos, Solid Lipid Nanoparticles (SLN), *Nanocomposite Mater. Biomed. Energy Storage Appl.*, IntechOpen (2022), <https://doi.org/10.5772/intechopen.102536>.
- [31] M. Calderone, E. Rodier, H. Lochard, F. Marciacq, J. Fages, A new supercritical co-injection process to coat microparticles, *Chem. Eng. Process. Process Intensif.* 47 (2008) 2228–2237, <https://doi.org/10.1016/j.cep.2007.12.001>.

- [32] E. Lepeltier, C. Bourgaux, P. Couvreur, Nanoprecipitation and the "Ouzo effect": Application to drug delivery devices, *Adv. Drug Deliv. Rev.* 71 (2014) 86–97, <https://doi.org/10.1016/j.addr.2013.12.009>.
- [33] M. Geszke-Moritz, M. Moritz, Solid lipid nanoparticles as attractive drug vehicles: Composition, properties and therapeutic strategies, *Mater. Sci. Eng. C.* 68 (2016) 982–994, <https://doi.org/10.1016/j.msec.2016.05.119>.
- [34] H. Behjati Rad, J. Karimi Sabet, F. Varaminian, Effect of Stearic Acid as a Co-solvent on the Solubility Enhancement of Aspirin in Supercritical CO₂, *Chem. Eng. Technol.* 42 (2019) 1259–1267, <https://doi.org/10.1002/ceat.201900043>.
- [35] D. Grooff, M.M. De Villiers, W. Liebenberg, Thermal methods for evaluating polymorphic transitions in nifedipine, *Thermochim. Acta.* 454 (2007) 33–42, <https://doi.org/10.1016/j.tca.2006.12.009>.
- [36] N. Garti, E. Wellner, S. Sarig, Effect of surfactants on crystal structure modification of stearic acid, *J. Cryst. Growth.* 57 (1982) 577–584, [https://doi.org/10.1016/0022-0248\(82\)90076-8](https://doi.org/10.1016/0022-0248(82)90076-8).
- [37] J.L.R. Arrondo, F.M. Goñi, J.M. Macarulla, Infrared spectroscopy of phosphatidylcholines in aqueous suspension a study of the phosphate group vibrations, *Biochim. Biophys. Acta (BBA)/Lipids Lipid Metab.* 794 (1984) 165–168, [https://doi.org/10.1016/0005-2760\(84\)90310-2](https://doi.org/10.1016/0005-2760(84)90310-2).
- [38] S.Y. Chan, Y.Y. Chung, X.Z. Cheah, E.Y.L. Tan, J. Quah, The characterization and dissolution performances of spray dried solid dispersion of ketoprofen in hydrophilic carriers, *Asian. J. Pharm. Sci.* 10 (2015) 372–385, <https://doi.org/10.1016/j.ajps.2015.04.003>.
- [39] E. Adeli, A comparative evaluation between utilizing SAS supercritical fluid technique and solvent evaporation method in preparation of Azithromycin solid dispersions for dissolution rate enhancement, *J. Supercrit. Fluids.* 87 (2014) 9–21, <https://doi.org/10.1016/j.supflu.2013.12.020>.
- [40] M.S. Kim, I.H. Baek, Fabrication and evaluation of valsartan-polymer-surfactant composite nanoparticles by using the supercritical antisolvent process, *Int. J. Nanomedicine.* 9 (2014) 5167–5176, <https://doi.org/10.2147/IJN.S71891>.
- [41] E. Reverchon, I. De Marco, Mechanisms controlling supercritical antisolvent precipitate morphology, *Chem. Eng. J.* 169 (2011) 358–370, <https://doi.org/10.1016/j.cej.2011.02.064>.
- [42] E. Reverchon, E. Torino, S. Dowy, A. Braeuer, A. Leipertz, Interactions of phase equilibria, jet fluid dynamics and mass transfer during supercritical antisolvent micronization, *Chem. Eng. J.* 156 (2010) 446–458, <https://doi.org/10.1016/j.cej.2009.10.052>.
- [43] E. Badens, Y. Masmoudi, A. Mouahid, C. Crampon, Current situation and perspectives in drug formulation by using supercritical fluid technology, *J. Supercrit. Fluids.* 134 (2018) 274–283, <https://doi.org/10.1016/j.supflu.2017.12.038>.